FLUIDIZED BED DRYING OF SOYBEAN MEAL: THE EFFECT OF DRYING KINETICS USING COMPUTATIONAL FLUID DYNAMICS

Alexandre M. S. Costa, amscosta@uem.br
Paulo R. Paraíso,
Luiz Mário M. Jorge,
Fernanda R. G. B. da Silva,
Universidade Estadual de Maringá Av. Colombo 5790, bloco 104 , Maringá, PR, 87020-900

Abstract. *In this work we investigate numerically the drying of soybean meal in a fluidized bed. Our modelling is implemented using the open-source code MFIX. For the code, the gas and solid phases are treated as inter-penetrating continua in an Eulerian framework Then, the locally-averaged (continuum) mass, momentum and energy balance, are solved using a modified version of the SIMPLE method. Here, we explore the effect of different parameters from drying kinetics on the results: inlet air condition, product mass, drying rate constant, equilibrium solids moisture. Towards validation of our modelling, the results are compared with a set of drying data for soybean meal from our experimental rig. The degree of accordance points to the better drying kinetics model to be used.*

Keywords*: fluidized bed, drying, computational fluid dynamics, MFIX*

1. INTRODUCTION

The fundamental goal during soybean meal production is a quality product with a minimum cost. The drying process contributes to final moisture approaches to the desired levels. Fluidized bed drying involves simultaneous heat, mass and momentum transfer process, giving a highly non-linear set of governing equations. Also numerous parameters affect drying processes, many of them material dependent. The process has a long record of theoretical models whose predictions have been wildly different from actual results, and equipment that has failed to meet its design specification. Industrial design manufacturers have tended to rely on empirical scale-up rules based on pilot-plant testing, rather than published theoretical models. The very limited acceptance of academic theories for drying by industrial users has also been due to bad experiences when attempts were made to use published theory for practical design (Mujumdar, 2006). In spirit of their large application, understanding of the complex multi-phase flows involved in fluidized beds using computer simulations can became a good approach to the design, optimization, and control of industrial-scale fluidized bed driers. Availability of more sophisticated computer models is expected to result in greatly increased performance and reduced costs associated with fluidized bed driers implementation and operation. In this work is explored the effect of different parameters from drying kinetics on the drying results predicted by a CFD code for a laboratory gas fluidized bed dryer.

2. EXPERIMENTAL SETUP

The experimental work was conducted at the Chemical Engineering Department of the Maringá State University. As shown in Fig. 1 the fluidized bed is composed of a cylindrical acrylic tube of 8.87 cm i.d. and 70 cm height. The air distributor is made of porous ceramic disc. A tap below the distributor is used to measure the air entering properties (temperature and relative humidity) by a digital psychrometer THWD-1 Amprobe Instruments. The pressure drop is measured by two pressure taps located right above the distributor and at the bed end. The air flow rate is controlled by three rotameters in parallel arrangement. The air is supplied by an industrial compressor and flow through an electrical resistance bank for heating.

The minimum fluidization velocity (u_{mf}) was 71 cm/s and was determined by the curve pressure drop versus air velocity according to procedure outlined in Foust (1980). The drying experiments were performed for a gas superficial velocity of 139 cm/s and for three different entering air temperatures : 25, 39 and 50 C. The mass of soybean meal used was 200 g corresponding to a 5 cm bed height. The initial moisture X_0 was 0.1993 g liquid water/g of moist soybean meal. The last value was obtained measuring the mass difference after drying the samples in a oven at 105 C for a 24 h period.

The soybean meal granulometric analysis was performed with sieves of 5, 6, 8, 12, 20 and 150 mesh. Approaching the industrial conditions, the soybean mean particles greater than 5 mesh size and smaller than 150 mesh size were disposed. Following the analysis, the calculated Sauter mean diameter was 0.1 cm. The density and packed bed voidage were determined simultaneously by adding a known mass of soybean meal in a beaker filled with a known volume of water. The displaced water volume corresponds to the volume of the particles, then the density is calculated by the quotient between mass and displaced volume. On the other hand, the quotient between volume of particles and volume of the bed gives the packed bed voidage of 0.346.

The experimental procedure is described next. Initially the flow rate was adjusted for the gas flowing through the empty tube. Next the gas inlet temperature was adjusted by controlling the dissipated power by the resistance bank. After that, the particulate is introduced by the top, beginning the data collection. The relative humidity of the exiting air were taken every 10 s and the inlet temperature and humidity was taken in the beginning and the end of each run.

The solid moisture $X_{s\text{-liquid water}}$ in the bed for a given time t can be obtained by using the exit air relative humidity UR data and a mass balance for the bed according to Eq. (1), where Q_0 is the air flow rate, ρ_{air} is the air density, P is the total pressure and P_{sat} is the gaseous water saturation pressure at exit temperature.

$$X_{s-liquid-water}(t) = X_0 - Q_0 \int_0^t \rho_{air} \frac{0.622\ UR\ P_{sat}}{P - UR\ P_{sat}} dt \tag{1}$$

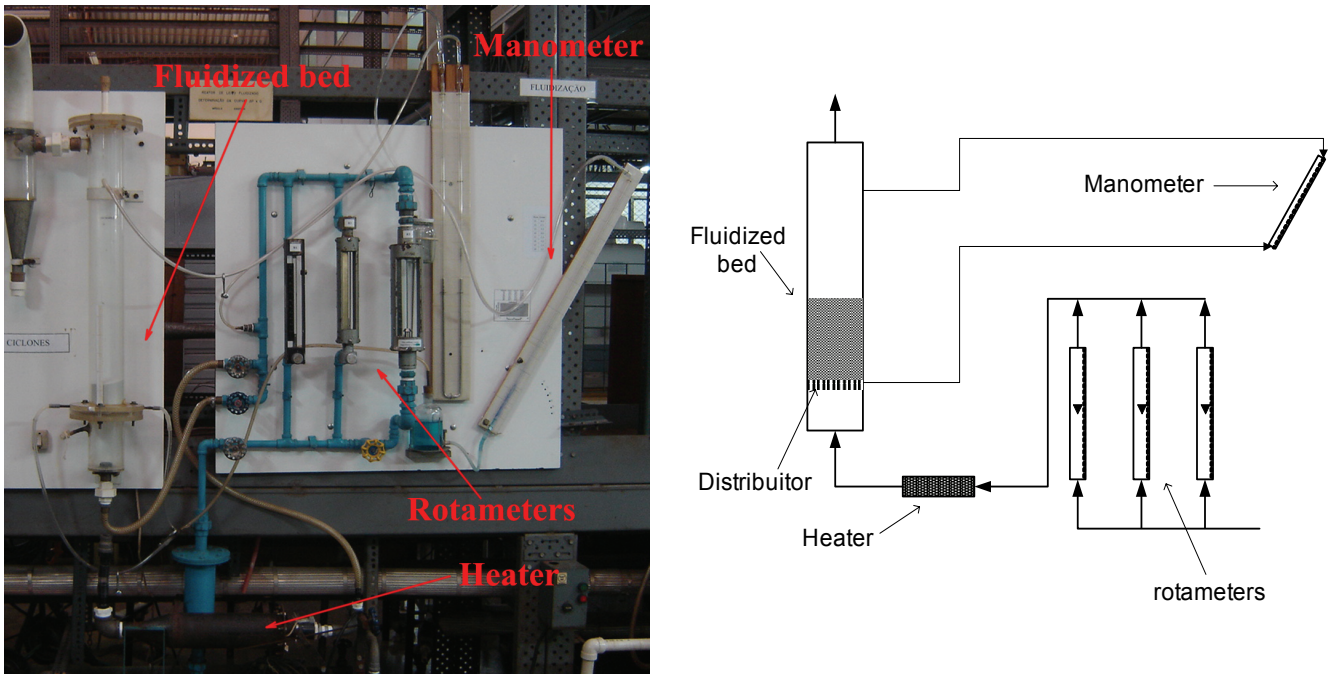

Figure 1. Experimental apparatus

3. TWO FLUID AND DRYING KINETICS MODEL

The mathematical model is based on the assumption that the phases can be mathematically described as interpenetrating continua; the point variables are averaged over a region that is large compared with the particle spacing but much smaller than the flow domain (see Anderson, 1967). A short summary of the equations solved by the numerical code in this study are presented next. Refer to Benyahia et al. (2006) and Syamlal et al. (1993) for more detailment.

The continuity equations for the fluid and solid phase are given by :

$$\frac{\partial}{\partial t}\left(\varepsilon_f \rho_f\right) + \nabla \bullet \left(\varepsilon_f \rho_f \vec{v}_f\right) = \sum_{n=1}^{N_f} R_{fn} \tag{2}$$

$$\frac{\partial}{\partial t}\left(\varepsilon_s \rho_s\right) + \nabla \bullet \left(\varepsilon_s \rho_s \vec{v}_s\right) = \sum_{n=1}^{N_s} R_{sn} \tag{3}$$

In the previous equations ε_f, ε_s, ρ_f, ρ_s, $\vec{v}_f$ and $\vec{v}_s$ are the volumetric fraction, density and velocity field for the fluid and solids phases. The right side term in the continuity equations accounts for interphase mass transfer because of chemical reactions or physical processes, such as evaporation. The subscript n corresponds to the n chemical specie.

The momentum equations for the fluid and solid phases are given by:

$$\frac{\partial}{\partial t}\left(\varepsilon_f \rho_f \vec{v}_f\right) + \nabla\bullet\left(\varepsilon_f \rho_f \vec{v}_f \vec{v}_f\right) = \nabla\bullet\bar{\bar{S}}_f + \varepsilon_f \rho_f \vec{g} - \vec{I}_{fs} \tag{4}$$

$$\frac{\partial}{\partial t}\left(\varepsilon_s \rho_s \vec{v}_s\right) + \nabla\bullet\left(\varepsilon_s \rho_s \vec{v}_s \vec{v}_s\right) = \nabla\bullet\bar{\bar{S}}_s + \varepsilon_s \rho_s \vec{g} + \vec{I}_{fs} \tag{5}$$

$\bar{\bar{S}}_f$ $\bar{\bar{S}}_s$ are the stress tensors for the fluid and solid phase. It is assumed newtonian behavior for the fluid and solid phases. Moreover, the solid phase behavior is divided between a plastic regime (also named as slow shearing frictional regime) and a viscous regime (also named as rapidly shearing regime). The constitutive relations for the plastic regime are related to the soil mechanics theory On the other hand, the viscous regime behavior is ruled by kinetic theory related parameters.

$\vec{I}_{fs}$ is the momentum interaction term between the solid and fluid phases. In his formulation there is a term proportional to velocities differences between phases: the drag coefficient β. There is a number of correlation the drag coefficient. The first of the correlations for the drag coefficient is based on Wen and Yu (1966) work. The Gidaspow drag coefficient is a combination between the Wen Yu correlation and the correlation from Ergun (1952). The correlation proposed by Syamlal and O'Brien (1993) carries the advantage of being adjustable for different minimum fluidization conditions. The drag correlation from Hill, Koch and Ladd (2001) work is based on Lattice-Boltzmann simulations. The blended drag correlation originally proposed by Lathowers and Bellan (2000) allows controlling the transition from the Wen and Yu, and Ergun based correlations.

Equation (5) is a transport equation for the granular energy Θ. Its solution provides a way of determine the pressure and viscosity for the solid phase during the viscous regime. The terms κ_s γ and ϕ_{gs} are the granular energy conductivity, dissipation and production, respectively.

$$\frac{3}{2}\left[\frac{\partial}{\partial t}\varepsilon_s \rho_s \Theta + \nabla\bullet\rho_s \vec{v}_s \Theta\right] = \bar{\bar{S}}_s : \nabla\vec{v}_s - \nabla\bullet\left(\kappa_s \nabla\Theta\right) - \gamma + \phi_{gs} \tag{6}$$

The energy equations in terms of temperatures T_f and T_s for the fluid and solid phases are given in Eqs. (7) and (8). The specific heat and conductive flux for the fluid and solid phase are denoted by C_{pf}, C_{ps}, $\vec{q}_f$ and $\vec{q}_s$, respectively. The second term in the right hand side of Eqs. (7) and (8) accounts for the thermal energy transfer between the phases. The last terms in Eqs (7) and (8) accounts for the enthalpy variation due to chemical or phase change reactions. For the energy equation the following assumptions were made : no viscous dissipation, no pressure work, no radiation exchange effects.

$$\varepsilon_f \rho_f C_{pf}\left[\frac{\partial T_f}{\partial t} + \left(\vec{v}_f \bullet \nabla\right) T_f\right] = -\nabla\bullet\vec{q}_f + \gamma_{fs}\left(T_s - T_f\right) - \Delta H_f \tag{7}$$

$$\varepsilon_s \rho_s C_{ps}\left[\frac{\partial T_s}{\partial t} + \left(\vec{v}_s \bullet \nabla\right) T_s\right] = -\nabla\bullet\vec{q}_s - \gamma_{fs}\left(T_s - T_f\right) - \Delta H_s \tag{8}$$

The species transport equations in terms of mass fractions X_{fn} and X_{sn} for the chemical species in the fluid and solid phases are given by Eqs. (9) and (10): In these equations the diffusive effects were neglected. The terms R_{fn} and R_{sn} represents the fluid and solids species production due to a chemical or phase change reaction. For our case of study, we considered the solid phase containing two species : liquid water and dry soybean meal. The fluid phase is considered composed of two species : gaseous water and dry air. The phase evaporation is modeled according to Eq. (11), where C_1 is an adjustable constant, and the superscript eq corresponds to the equilibrium values.

$$\frac{\partial}{\partial t}\left(\varepsilon_f \rho_f X_{fn}\right) + \nabla\bullet\left(\varepsilon_f \rho_f \vec{v}_f X_{fn}\right) = R_{fn} \tag{9}$$

$$\frac{\partial}{\partial t}\left(\varepsilon_s \rho_s X_{sn}\right) + \nabla\bullet\left(\varepsilon_s \rho_s \vec{v}_s X_{sn}\right) = R_{sn} \tag{10}$$

$$R_{s-liquid-water} = C_1\left(X_{\text{s-liquid water}} - X^{eq}_{\text{s-liquid water}}\right) \tag{11}$$

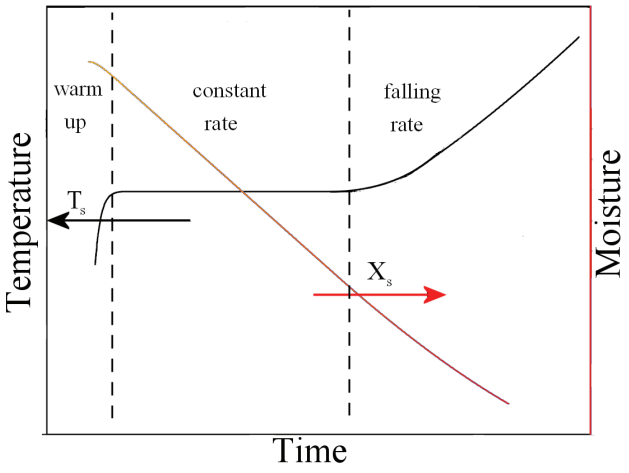

Figure 2. Trends during fluidized bed drying

To better understand the impact of moisture on fluidized bed drying processes, a brief review of drying fundamentals is justified. The characteristic drying curve of drying a batch of solids is presented in Fig. 2. The three distinct periods: (a) the warming-up period, (b) the constant-rate period where moisture evaporates from the saturated surface of the solids and (c) the falling-rate period. In periods a and b, drying is controlled entirely by the rate of heat and mass transfer between the particle and drying medium, i.e., by the external drying conditions. In these periods, the wet particle is quickly warmed up to the wet-bulb temperature of the drying air and the temperature is kept constant until the end of the constant-rate period. It should be noticed also that during the constant period the heat from the air is equal to the water latent heat, and acts to evaporate the water from the particle surface.

As the moisture content of the solids decreases past a certain point, the rate of drying starts to decline as rightly. This transition point, indicated as the critical moisture content, occurs when an unceasing film of moisture cannot be supplied on the surface of the particles. In porous media, the critical point is achieved when the rate of moisture removal from the particle does not equal the rate of evaporation under saturation conditions. For non-porous solids, this takes place when the solids are dry. Once the critical moisture content is exceeded, the migration of water from within the porous solids does not allow heat transfer conditions to reach a steady state. This result in an increment in the product and exhaust gas temperatures over the saturation temperature of the inlet gas. This drying regime is designated the falling rate period. We verified experimentally that for the soybean meal the period for the constant rate regime is the dominant.

4. NUMERICAL METHOD

MFIX (Multiphase Flow with Interphase eXchanges) is an open source CFD code developed at the National Energy Technology Laboratory (NETL) for describing the hydrodynamics, heat transfer and chemical reactions in fluid-solids systems. It has been used for describing bubbling and circulating fluidized beds, spouted beds and gasifiers. MFIX calculations give transient data on the three-dimensional distribution of pressure, velocity, temperature, and species mass fractions.

The hydrodynamic model is solved using the finite volume approach with discretization on a staggered grid. A second order accurate discretization scheme was used and superbee scheme was adopted for discretization of the convective fluxes at cell faces for all equations in this work. With the governing equations discretized, a sequential iterative solver is used to calculate the field variables at each time step. The main numerical algorithm is an extension of SIMPLE. Modifications to this algorithm in MFIX include a partial elimination algorithm to reduce the strong coupling between the two phases due to the interphase transfer terms. Also, MFIX makes use of a solids volume fraction correction step instead of a solids pressure correction step which is thought to assist convergence in loosely packed regions. Finally, an adaptive time step is used to minimize computation time. See Syamlal (1998) for more details.

In this work, the parameters for controlling the numerical solution (e.g., under-relaxation, sweep direction, linear equation solvers, number of iterations, residual tolerances) were kept as their default values. For setting up the mathematical model we also kept the default values.

Figure 3 shows the initial and boundary conditions for the numerical simulations. The numerical runs were based on an axisymmetric cylindrical coordinate system. The grid employed after mesh refinement studies were 20 (radial) × 80 (axial) cells. When not differently specified the height taken for the dense bed was 5 cm. Each simulation was taken for a 300 s simulation time. The computer used in the numerical simulations was a PC with OpenSuse linux and Intel Quad Core processor.

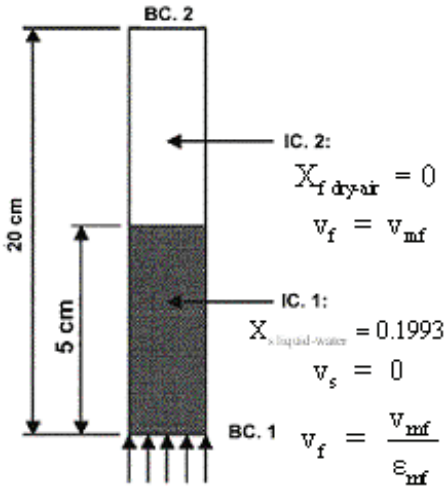

Figure 3. Initial conditions (IC) and boundary condition (BC) for CFD simulations.

5. RESULTS AND DISCUSSION

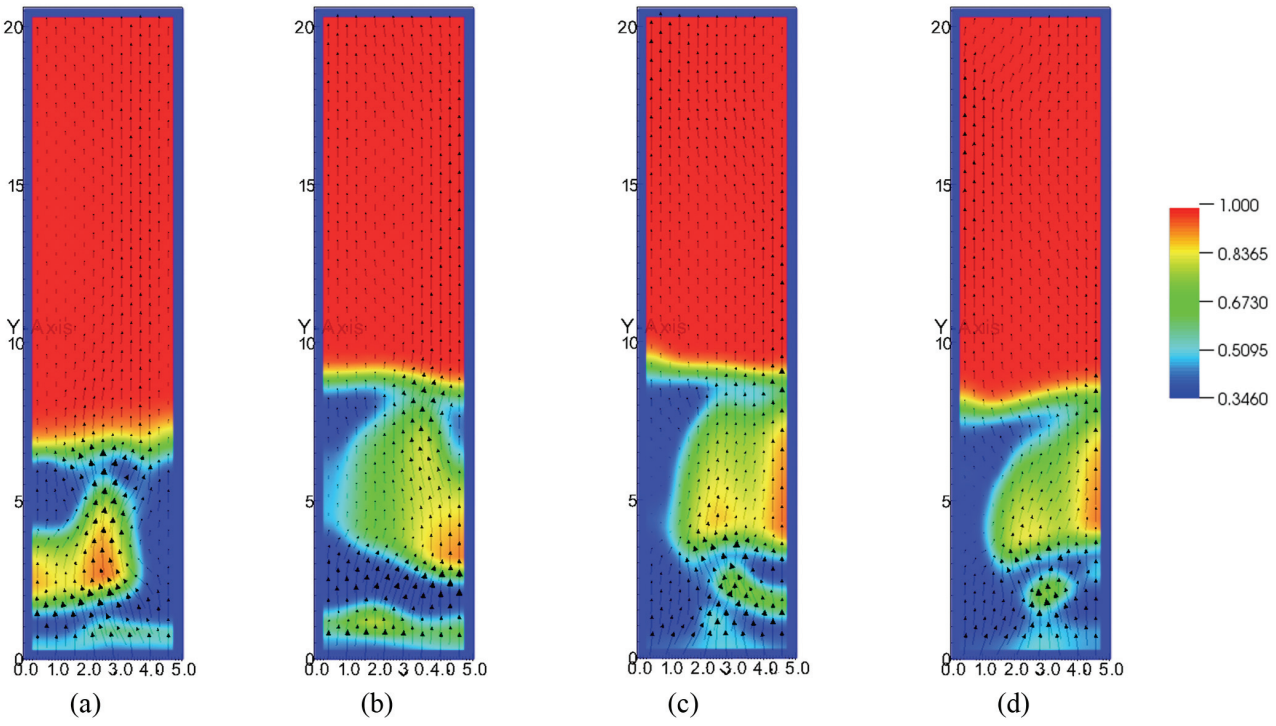

Figure 4. Instantaneous velocity and voidage fields by CFD. (a) 20.0 s, (b) 20.2 s, (c) 20.4 s, (d) 20.6 s

Figure 4 is a sampling plot showing the instantaneous gas velocities and gas volumetric fraction fields for different times. It clearly shows the high voidage regions (bubbles) in the dense part of the bed .

The effect of changes on simulation parameters for the drying kinetics model on the final drying results is presented next. All the time results for drying will be given in terms of an averaged radial and for a given axial position in the dense part of the fluidized bed. For the varying axial results, it was taken radial and time-averaged values.

Figure 5(a) shows the effect of drying intensity on the solids temperature in the dense bed. As it can be seen from Fig. 5 (a), ten times greater drying rate coefficient result in a more intense degree of initial temperature decaying. It also must be pointed the slight trend of temperature increase after reaching the minimum value. This is also verified by our experiments. Figure 5(b) shows the effect of drying rates coefficients on the time varying water mass fraction in the solid phase. As it can be seen the rate of moisture decreases is more intense for the higher C_1 coefficient.

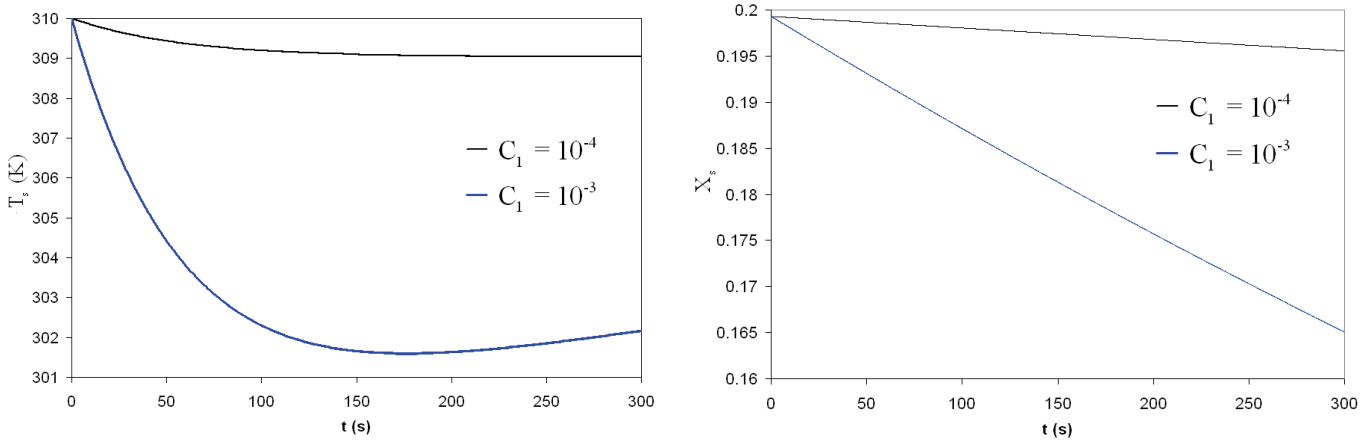

(a) (b)

Figure 5. Effect of different drying rates coefficients on the numerical results for (a) solids temperature in the dense and (b) water mass fraction in solids

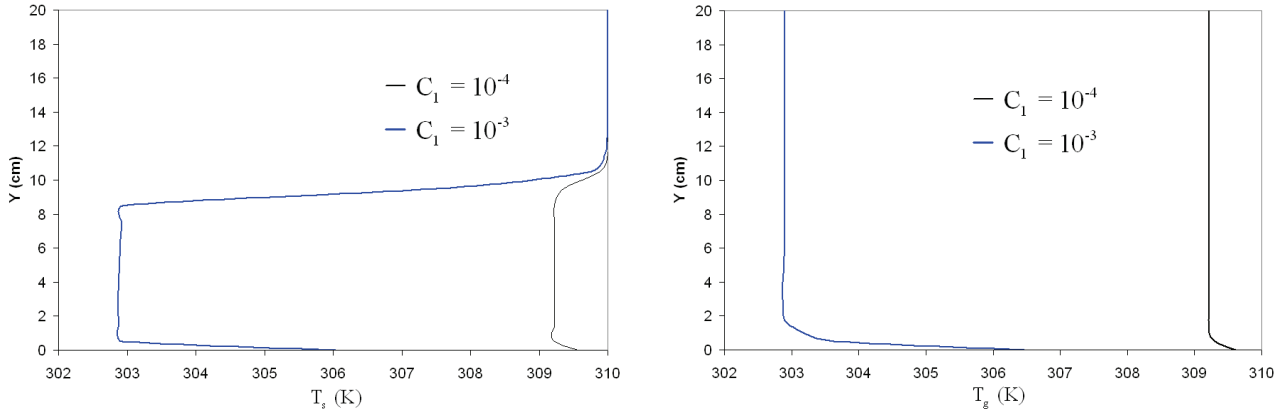

(a) (b)

Figure 6. Effect of different drying coefficients on the time and radial averaged temperature axial profile for phases (a) solid and (b) gas.

Figure 6 shows the effect of the drying coefficients in the axial profiles for temperatures. It must be pointed out that results for the solids are meaningful only for the dense portion of the bed. As already shown in Fig. 5 the temperature decrease is more intense for the highest drying coefficient.

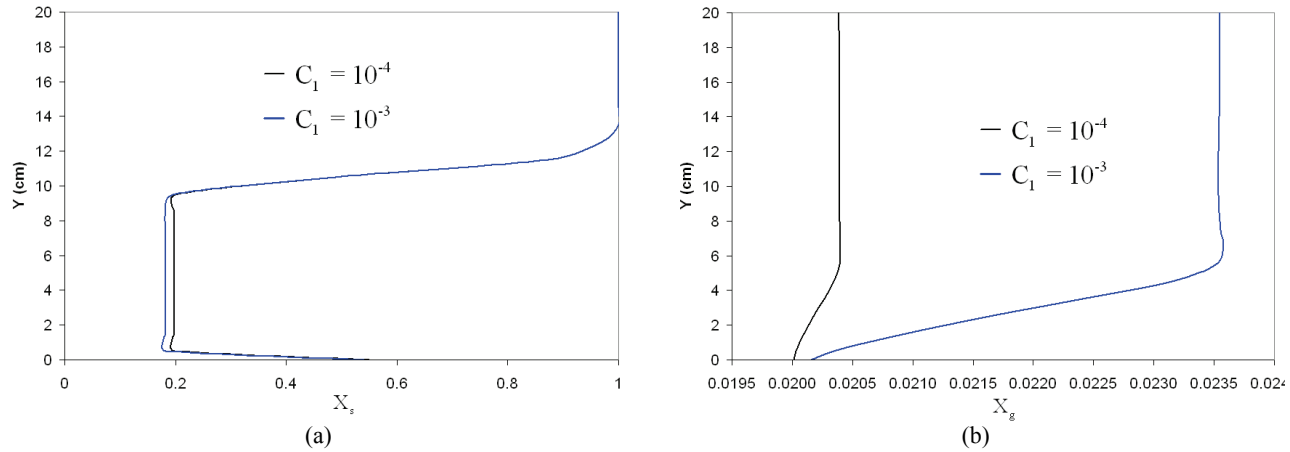

(a) (b)

Figure 7. Effect of different drying coefficients on the timely and radial averaged water mass fraction axial profile for phases : (a) solid and (b) gas.

Figure 7 shows the effect of drying coefficients on the predicted water mass fraction profiles. Comparison of the scales of Fig. 7(a) e 7(b) shows that although the degree of difference is more noticeable for the water mass fraction in the gas phase, the same degree of difference is predicted by solids phase. As shown for temperature profiles, the results for solids are only meaningful for the dense part of the bed, i.e., lower heights.

In the next figures, it is shown the effect of different values for the solids equilibrium moisture content in solids. The values used were chosen in a range around the actual measured value reported from experiments. Figure (8)a shows the effect on the bed temperature as function of time. The difference in curves for Figure (8) can be interpreted in terms of the drying driving potential being more intense for the lowest value of equilibrium moisture content in solids, in this way resulting in a more intense temperature reduction. As already verified for Figure (5), in Figure (8)a there is also a slight solids temperature increase after the minimum value is reached. Figure 8b shows the results for the water mass fraction in solid phase for the dense bed as function of time. From figure (8)b shows the tendency of moisture decrease more intense for the lowest equilibrium moisture content.

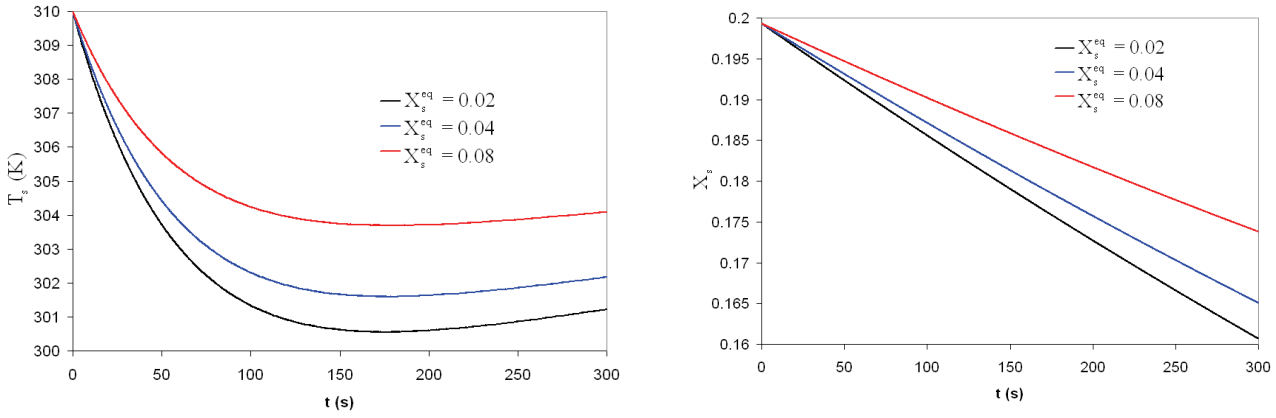

(a) (b)

Figure 8. Effect of equilibrium moisture content on : (a) bed temperature value and (b) the predicted water mass fraction in phase solid

Figures (9) and (10) shows the effect of equilibrium moisture value on the axial profiles for temperature and water mass fraction. Analyzing Figure (9)a and (9)b, its is verified the same predicted temperature for both phases in the dense bed and the gas phase temperature is kept constant after the dense bed. Figure 10 (a) and 10 (b) from water mass fraction in the phases. Comparison with Figure 7, shown the influence in the axial profile is also small for the variation of the equilibrium moisture content.

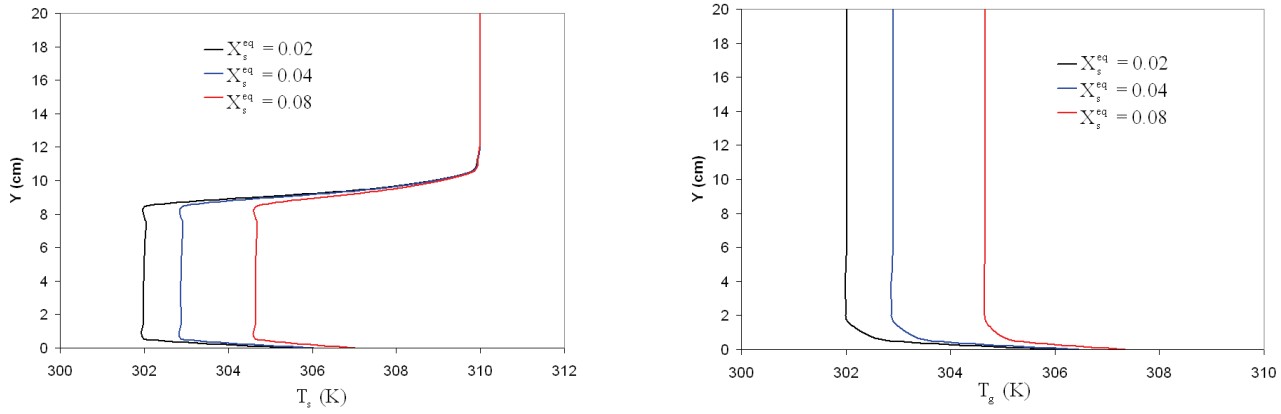

(a) (b)

Figure 9. Effect of equilibrium moisture content on the time and radial averaged temperature axial profile for phase : (a) solid and (b) gas.

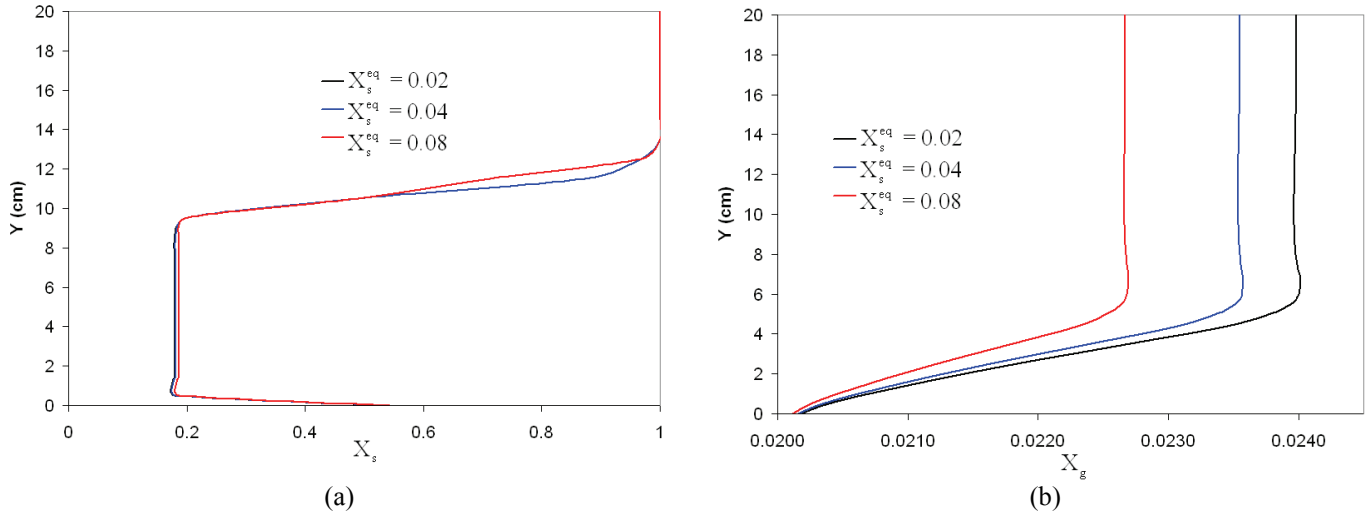

(a) (b)

Figure 10. Effect of equilibrium moisture content on on the timely and radially averaged water mass fraction axial profile for phases : (a) solid and (b) gas.

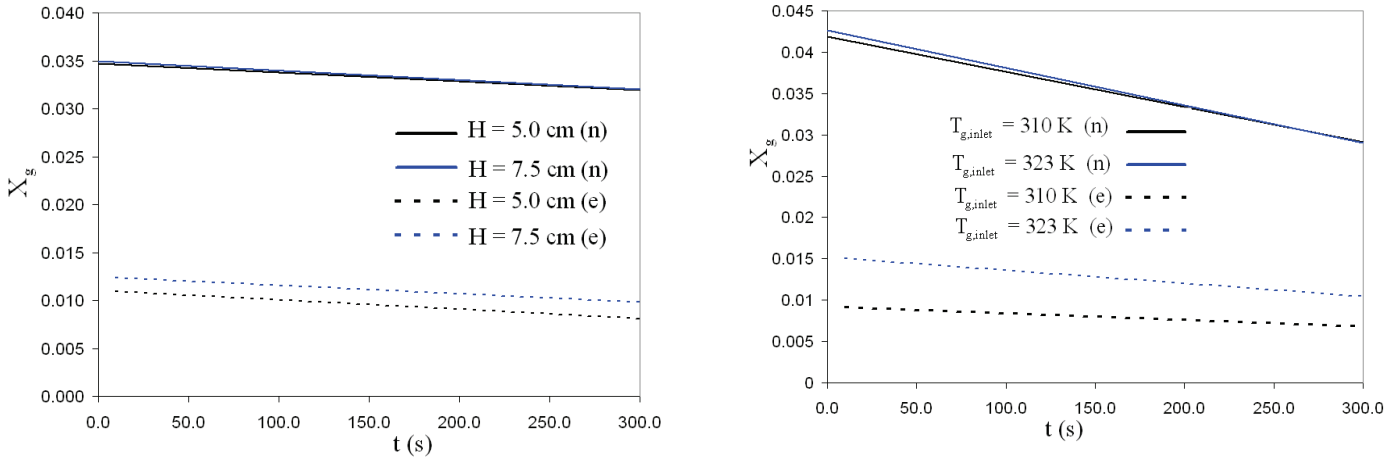

(a) (b)

Figure 11. Experimental water mass fraction in gas phase measured in the freeboard as function of time for different bed loads (a) and inlet gas temperatures (b) for V = 173 cm/s

Figure 11 shows a comparison with the experimental values of Xg (taken from the UR values of air at exit) and the numerical simulation results. Although the experimental results were taken for a longer period we only based our comparisons in a 300 s period. This is justifiable because longer simulations increase expensively the computational time. Figure 11(a) shows the comparison for two different bed heights at a fixed inlet air velocity, where the solid lines correspond to the numerical values and the dotted lines to the experimental values. Analyzing Figure (a) we can observe the values predicted by the numerical model are greater than the experimental. On the other side, the trends in the Xg decaying with time, i.e., the inclination of experimental and numerical lines are very close. Although the experimental values showed a difference in the Xg values with the bed height this difference is small. In this sense, the numerical values that did not predict difference in the results with the bed height are in good agreement with the experimental values. Figure 11(b) shows the comparison between numerical (n) and experimental (e) values for two different inlets temperatures at a fixed air inlet velocity. As in Figure 11(a) the numerical model is over predicting the water mass fraction. The inclination in the numerical lines is greater suggesting that the degree of over prediction is diminishing for longer periods of time. The variation of the results with the air inlet temperature shown by the experimental lines is only slightly shown for the numerical values during the initial period. The trend of decaying with time is followed by both experimental and numerical values. This discrepancy suggest a number of causing factors for being investigated further, such as, improvement in the evaporation model (Eq. 11) and bed hidrodynamics parameters.

6. CONCLUSIONS

The available mathematical model and numerical code were used to predict the hydrodynamics and drying kinetics for drying of soybean meal in a fluidized bed. In this work the numerical results points to sensitivity for parameters of the drying kinetics model. The results are sensitive to the drying rate coefficient C1, with a more intense degree of solids moisture decreasing for a greater value of C1. The solids temperature variation trend with time captured by the numerical model is in accordance with our experimental evidences. The numerical solution also predicts a greater value of solids temperature decrease with time for the greater value of C1. The influence of C1 is also observed in the time averaged axial profiles. The influence of the equilibrium moisture content on the numerical results points to greater degree of moisture decrease for the lower values of X_s^{eq}. The solids temperature decrease with time is also greater for the lower value of X_s^{eq}. Similar influence is also verified for the axial profiles for solids temperature and moisture content. Finally, a comparison with a set of experimental results from our lab scale fluidized bed dryer shows some agreement in trends. The disagreement in the magnitude between experimental and numerical values tips for further refinement in the drying kinetics model and parameters from hidrodynamics.

7. ACKNOWLEDGEMENTS

The support from MFIX users forum and CENAPAD-SP is gratefully acknowledged

8. REFERENCES

Anderson, T. B., 1967, “A fluid mechanical description of fluidized beds: Equations of motion”, Industrial Engineering Chemical Fundamentals, Vol 6, pp. 527-539.

Benyahia, S., Syamlal, M., O’Brien, T. J., “Summary of MFIX Equations 2005-4”, 1 March 2006: <http://www.mfix.org/documentation/MfixEquations2005-4-1.pdf>.

Ergun, S., 1952, “Fluid-flow through packed columns”, Chemical Engineering Progress, Vol 48, n. 2, pp. 91-94.

Foust, A. S., 1980, “Principles of Unit Operations”, Wiley, N. York, USA, 768 p.

Hill, R. J., Koch, D. L., Ladd, J. C., 2001, “Moderate-Reynolds-number flows in ordered and random arrays of spheres”, Journal of Fluid Mechanics, Vol 448, p. 243-278.

Hill, R. J., Koch, D. L., Ladd, J. C., 2001, “The first effects of fluid inertia on flows in ordered and random arrays of spheres”, Journal of Fluid Mechanics, Vol 448, pp. 213-241.

Lathowers, D., Bellan, J., 2000, “Modeling of dense gas-solid reactive mixtures applied to biomass pyrolysis in a fluidized bed”, Proceedings of the 2000 U.S. DOE Hydrogen Program Review, NREL/CP-570-28890. USA.

Mujumdar, A. S., 2006, “Handbook of Industrial Drying”, CRC, N. York, USA, 1312 p.

Syamlal, M., 1998, “MFIX Documentation, Numerical Techniques”, Technical Note, DOE/MC-31346-5824, NTIS/DE98002029, National Technical Information Service, Springfield, VA, USA.

Syamlal, M., Rogers, W. A., O’Brien, T. J., 1993, “MFIX Documentation, Theory Guide”, Technical Note, DOE/METC-94/1004, NTIS/DE94000087, National Technical Information Service, Springfield, VA, USA.

Wen, C. Y., Yu, Y. H., 1966, “Mechanics of Fluidization”, Chemical Engineering Progress Symposium Series, Vol 62, n. 62, pp. 100-111.

5. RESPONSIBILITY NOTICE

The authors are the only responsible for the printed material included in this paper.